Applied Physics B (2019) 125:32
https://doi.org/10.1007/s00340-018-7126-3

Applied Physics B
Lasers and Optics

Thermally guided Yb-doped fiber-rod amplifier and laser

C. R. Smith[1] · N. Simakov[1,2] · A. Hemming[2] · W. A. Clarkson[1]

Received: 1 July 2018 / Accepted: 16 December 2018

Abstract
In this paper, we describe a thermally guided fiber-rod amplifier and laser oscillator, which exploit thermal guiding to achieve mode control. This power scalable approach operates with mode sizes that are typically an order of magnitude larger than traditional single-mode fibers. Operating as an amplifier, we achieve a small-signal gain of 5 dB at 1030 nm whilst maintaining excellent beam quality ($M^2 < 1.1$). In a laser configuration, we obtained 13.1 W of diffraction-limited ($M^2 < 1.1$) output power at 1032.5 nm, with a slope efficiency 53% with respect to absorbed power. A model predicting beam evolution through the thermally guided fiber-rod gain medium is presented and validated.

1 Introduction

Lasers with high average power, high peak power, large pulse energy, excellent beam quality, and high efficiency are sought after for numerous applications including materials processing, defence, and scientific research. These desirable attributes can be provided by solid-state lasers which provide a versatile source of laser radiation. Broadly, solid-state architectures can be divided into bulk and fiber geometries. Within a bulk architecture, the resonator design dictates the size of the free-space laser mode, whilst in a fiber, the guided mode is defined by the engineered refractive index profile.

The prevalent bulk rod laser can deliver high peak power and high pulse energy, but is limited in average output power by deleterious thermal effects. For example, thermal lensing can lead to aberration of the fundamental laser mode and/or multimode operation degrading beam quality. Furthermore, although kW-level average power operation has been achieved, beam quality is heavily compromised, suggesting that fundamental mode operation is generally limited to the 100 W level [1, 2]. The extreme geometry of optical fibers provides a large surface area-to-volume ratio, allowing these devices to display excellent thermal management properties. Furthermore, fiber lasers have reached the 10 kW average power level with diffraction-limited beam quality [3]. However, the tight beam confinement and long interaction length favours nonlinear effects which can be very detrimental to performance. In addition, high intensities can lead to laser-induced damage of the fiber core. These effects are especially problematic in pulsed systems, severely limiting the peak power and pulse energy that can be generated.

Consequently, increasing beam size within the fiber whilst maintaining single-mode guidance is desirable for obtaining higher peak powers and pulse energies. A larger beam will result in a lower intensity for a given power, thus increasing the threshold power for the onset of nonlinear effects and laser-induced damage. Furthermore, a larger mode size results in a higher saturation energy and, therefore, a higher extractable pulse energy. However, a larger core must be accompanied with a lower numerical aperture (NA) to maintain single-mode guidance. This approach cannot be applied indefinitely, since a lower NA results in weaker guiding. One can circumvent this limitation by utilising a slightly multimode fiber with an appropriate degree of bending to ensure higher order modes experience a significantly higher loss than the fundamental mode, which becomes the only excited mode. This approach has been employed in a fiber with a 40 µm core diameter to achieve an average power of 1.36 kW in a near diffraction-limited beam [4]. Alternative designs such as microstructured fibers allow the realisation of large core low NA devices. For example, 830 W was obtained for 640 fs pulses at 78 MHz [5], whilst a fiber with a 108 µm diameter core achieved a peak power of 3.8 GW for 480 fs pulses [6]. Another concept is the single-crystal fiber which

✉ C. R. Smith
crs1g08@soton.ac.uk

[1] Optoelectronics Research Centre, University of Southampton, Southampton SO17 1BJ, UK

[2] Laser Technologies Group, Cyber and Electronic Warfare Division, Defence Science and Technology Group, Edinburgh, SA 5111, Australia

Published online: 04 February 2019

guides pump radiation, whilst the large signal mode propagates freely. However, poor beam quality is typical of these devices, with 250 W achieved in a highly multimode beam ($M^2 \approx 15$) [7].

In light of these limitations, we have investigated an alternative strategy for power scaling based on the use of thermal guiding as the means for mode selection in a fiber gain element. The use of thermal guiding as the guidance mechanism in Yb-doped index-antiguiding-core fibers has been reported in [8], and numerical studies on single-mode operation of a thermally guided large-mode-area fiber amplifier are reported in [9]. In this contribution, we investigate a 'fiber-rod' geometry with a much larger Yb-doped core and a much shorter device length. This approach which we refer to as a thermally guided fiber-rod (TGFR) laser occupies the domain between bulk rod and traditional fiber lasers. The TGFR consists of a rare-earth-doped core, with a diameter on the order of hundreds of microns, and a lower refractive index cladding layer, with a diameter on the order of hundreds of microns to a millimetre. The length of the TGFR is typically a few centimetres to a few tens of centimetres. The key novelty of the TGFR laser is its unique method of mode control, which utilises thermally induced lensing to elegantly control the laser mode size along the device.

The TGFR laser is a power scalable concept, which aims to achieve high average and/or peak power, large pulse energy, and excellent beam quality by combining the advantages of rod and fiber lasers whilst avoiding their limitations. The large beam size compared to traditional fiber lasers, combined with the relatively short length, ensures that the TGFR has a higher threshold for deleterious nonlinear effects and optical damage. The larger mode area will ultimately allow higher pulse energies to be extracted from the device. Unlike traditional bulk rod devices, the TGFR utilises the key thermal management advantage of the fiber geometry by maintaining a high aspect ratio.

This paper investigates the underlying principles of operation of the TGFR in the continuous-wave regime for amplifier and laser oscillator configurations, as a proof of concept. A simple theoretical model for mode propagation in the TGFR is developed and validated in experimental studies for an extra-large core Yb-doped fiber-rod. Finally, the prospects for further power scaling whilst maintaining diffraction-limited single-mode beam quality are considered.

2 Thermally induced guiding mechanism

Rare-earth ion-doped silica was deemed an excellent candidate for demonstrating the TGFR concept, owing to its high fracture limit combined with well-established fabrication techniques for producing high purity material with exceptionally low background loss, paving the way for high power

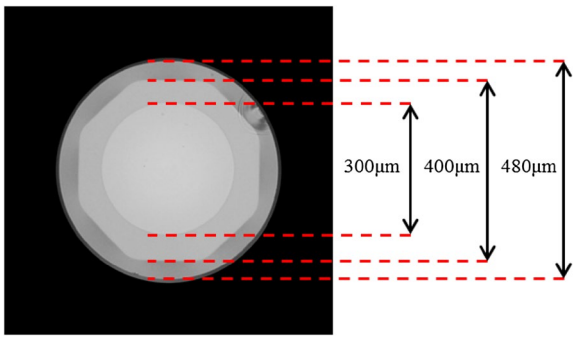

Fig. 1 TGFR cross section

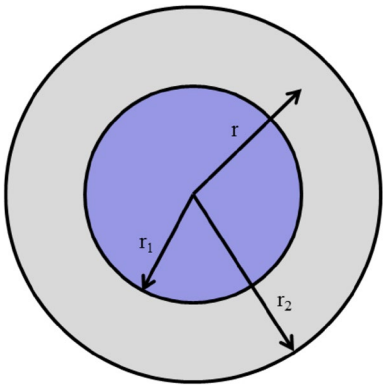

Fig. 2 TGFR cross section

operation. Crucially, this material has a positive thermo-optic coefficient, dn/dT, which is an essential requirement for the thermally induced guiding mechanism. An extra-large-mode-area silica fiber supplied by Nufern was thus selected for the demonstration. The all-glass fiber (cross section shown in Fig. 1) consisted of a 300 µm diameter core with an NA of 0.11 doped with Yb_2O_3, a 400 µm flat-to-flat octagonal inner-cladding with an NA of 0.22, and a 480 µm diameter outer-cladding. The preform was fabricated by Heraeus using powder sinter technology as outlined in [10].

Figure 2 shows the cross section of the TGFR, where r represents the radial coordinate. Here, we have considered the TGFR to consist of two regions, namely, the core region, radius r_1, and the cladding layer, with radius r_2. The TGFR will guide signal radiation entirely within the core, whilst pump radiation may be guided within the core or cladding layer. Pump power is absorbed in the core region and a fraction of this power is converted to heat.

To model guiding, it is necessary to have a knowledge of the value of the refractive index, n, within the core region as a function of radial position, r, and longitudinal position, z. It is assumed that perturbations to the refractive index can arise due to heating of the material from absorbing pump radiation, and from an inherent static contribution that is

built in to the TGFR as a result of the fabrication process. In this analysis, we ignore the large change in refractive index at the core-cladding boundary, since the mode size solutions of interest are small compared to the core diameter. Both these contributions are assumed to be parabolic in nature, with the highest value, n_0, at the centre of the TGFR. This scenario can be described in the following equation:

$$n(r,z) = n_0(z) - \frac{1}{2}n_g(z)r^2, \tag{1}$$

where n_g represents the rate of change of refractive index with radial distance at a particular longitudinal position. As discussed, n_g comprises of a thermal, n_t and static, n_s, component:

$$n_g(z) = n_t(z) + n_s. \tag{2}$$

Here, we assume that the thermal component is a function of z, since the pump deposition density depends on longitudinal position, whilst the static component is considered constant along the device. One can consider the device as consisting of an infinite number of infinitesimally thin longitudinal slices of thickness dz. Therefore, pump absorption across a slice can be approximated as constant, and the thermal component can be derived from the temperature distribution in a cylindrical rod geometry [11] and Eqs. (1) and (2) as

$$n_t(\mathrm{d}z) = \frac{\mathrm{d}n}{\mathrm{d}T}\left(\frac{P_H}{2\pi r_1^2 \kappa \mathrm{d}z}\right), \tag{3}$$

where dn/dT is the thermo-optic coefficient of the material, P_H is the heat power deposited in a slice, and κ is the thermal conductivity of the material.

P_H is related to the pump power, $P_p(z)$, at position z:

$$P_H = -\left(\gamma_H \frac{\mathrm{d}P_p(z)}{\mathrm{d}z}\right)\mathrm{d}z, \tag{4}$$

where γ_H is the fraction of absorbed pump power converted to heat.

One can model the guiding effect using Gaussian beam propagation combined with ABCD matrix formalism. Using the equation:

$$q_{out} = \frac{Aq_{in} + B}{Cq_{in} + D}, \tag{5}$$

where $q_{in/out}$ is the complex beam parameter of the input/output beam of each slice. The relevant ABCD matrix describing a slice of medium governed by Eq. 1 is given by [11]

$$\begin{pmatrix} A & B \\ C & D \end{pmatrix} = \begin{pmatrix} \cos\left(\mathrm{d}z\sqrt{\frac{n_g}{n_0}}\right) & \frac{1}{\sqrt{n_0 n_g}}\sin\left(\mathrm{d}z\sqrt{\frac{n_g}{n_0}}\right) \\ -\sqrt{n_0\, n_g}\sin\left(\mathrm{d}z\sqrt{\frac{n_g}{n_0}}\right) & \cos\left(\mathrm{d}z\sqrt{\frac{n_g}{n_0}}\right) \end{pmatrix}. \tag{6}$$

Furthermore, one can use the output beam parameters produced from one slice as the input to the next. This allows the output beam properties after any number of slices, and hence the guiding nature of the device, to be predicted, assuming knowledge of the relevant parameters.

To illustrate the impact of thermal guiding on mode size evolution, Fig. 3 depicts several examples, where we consider the guiding to be purely thermal in nature. Here, we assume a simplified case, where pump power is absorbed uniformly within the core region of a 10 cm long section of the demonstration material, as shown in Fig. 1. The pump wavelength is 915 nm and the signal wavelength is 1030 nm. It is assumed that the device is water-cooled. Values for the thermal conductivity and thermo-optic coefficient for silica fibers are taken from [12, 13] as 1.38 W m^{-1} K^{-1} and 12.9×10^{-6} K^{-1}, respectively. In this uniform heat deposition scenario, it is possible to launch a beam size, such that the diffraction of the beam is perfectly balanced by the focusing of the thermally induced guide, resulting in a perfectly guided beam which does not vary in size along the device length. One can show that, by stipulating $q_{in} = q_{out}$, the beam size that satisfies this condition, w_G, is described by

$$w_G = \left(\frac{\lambda^2}{\pi^2 n_0 n_t}\right)^{1/4}, \tag{7}$$

where λ is the signal wavelength. By comparing Eqs. 3 and 7, we can see that

$$w_G \propto \left(\frac{1}{P_H}\right)^{1/4}. \tag{8}$$

Thus, as one would expect, an increase in absorbed heat power results in a smaller guided beam size. This highlights an important power-scaling feature of the TGFR, namely, that the heat power absorption can be tailored by varying the TGFR doping concentration and/or core/cladding area ratio to ensure the guided beam size is suitable, i.e., the beam does not become too small as a result of excessive heat loading. This also means that the TGFR length would have to be scaled accordingly to maintain high pump absorption efficiency. Thus, scaling power in the TGFR, whilst maintaining a relatively large beam size and high overall efficiency, should be quite straightforward.

The first scenario in Fig. 3 considers launching a 100 µm beam waist on the TGFR input face. The beam is initially focused by the parabolic refractive index profile. However, a smaller beam has a higher tendency to diffract, and therefore, the beam forms a waist of 30.6 µm before expanding. In contrast, a larger beam is more sensitive to lensing; therefore, the beam reaches a maximum of 100 µm before being focused again in an identical manner. The beam repeats this oscillation along the length of the device with a period of

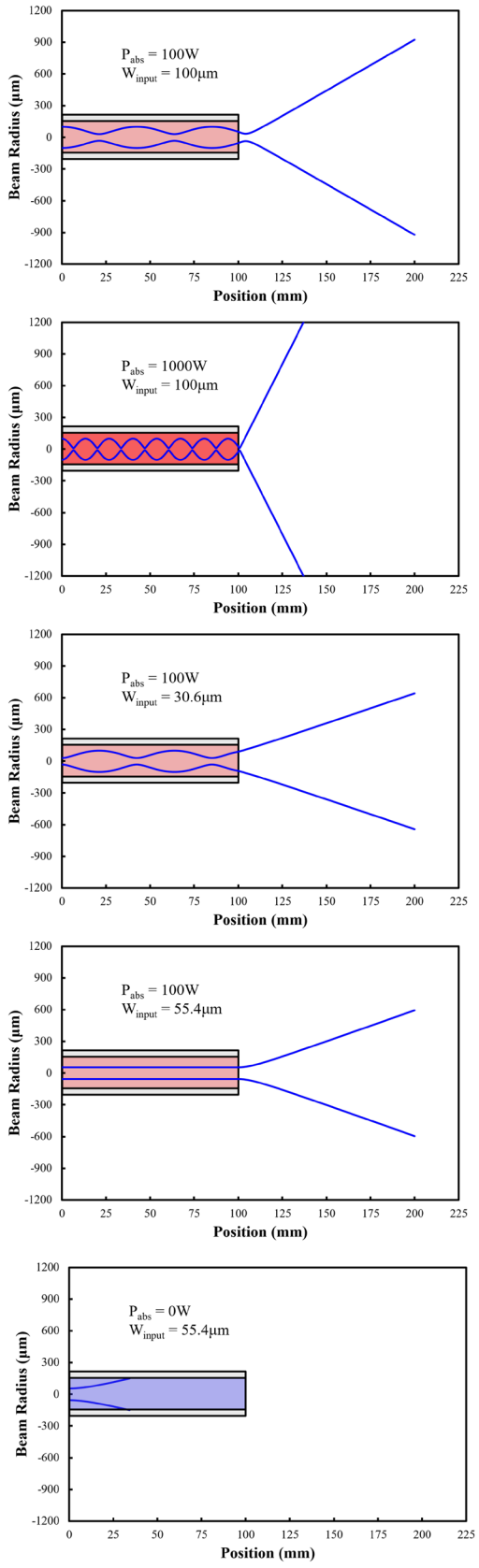

Fig. 3 Beam evolution for scenario 1 (top) to 5 (bottom)

42.6 mm. A simple argument based on equating the two sides of Eq. 4 shows that the beam oscillation period is proportional to $1/\sqrt{P_H}$. Thus, if 1000 W were absorbed in the device, (i.e., a tenfold increase), the period would decrease by $1/\sqrt{10}$, to a value of 13.5 mm. The beam waist radius within the device would also decrease owing to the stronger thermal lens. In fact, the product of the maximum and minimum beam radii is also proportional to $1/\sqrt{P_H}$; hence, the beam waist would reduce to approximately 9.5 µm, as shown in the second scenario. The third scenario assumes the original absorbed pump power of 100 W, but instead launches a beam waist of 30.6 µm. The period and product of the maximum and minimum beam radii are independent of the input waist parameters; therefore, the beam oscillates out of phase with scenario 1. By stipulating an equal beam waist at the input and output of the device, i.e., Equation 7, we see that the perfectly guided beam will have a radius of 55.4 µm, as shown in the fourth scenario. Finally, the fifth scenario shows the situation, where the same input beam from scenario 4 is launched into a device, where no pump power is absorbed and we assume no static contribution. Thus, the beam experiences diffraction with no focusing and consequently interacts with the edge core/cladding interface after approximately 34 mm, where the beam would be guided by the engineered step-index guide. This interaction leads to a degradation of beam quality and the formation of a non-Gaussian beam profile. In this scenario, the mode size is no longer small compared to the core diameter; thus, our approach based on beam propagation through the ABCD matrix given in Eq. 5 is no longer a valid description. Note that we have not included the non-Gaussian beam propagation after the interaction point in scenario 5.

The scenarios in Fig. 3 show the TGFR operating in a single-pass amplifier configuration. When considering a laser design, it is important to ensure operation on the fundamental mode. The simplest resonator design would be to butt-couple appropriate mirrors to the end-faces of the TGFR device to construct a cavity. This concept is shown in Fig. 4a, where a mirror with high transmission (HT) at the pump wavelength and high reflectivity (HR) at the lasing wavelength is positioned at the pump input end, and an output coupler mirror at the lasing wavelength is positioned at the output end. This design does not provide feedback discrimination for different modes, ensuring that each mode has essentially the same high feedback efficiency. Therefore, one would expect to obtain a highly multimode output beam from this resonator, since the core of the TGFR can support numerous transverse modes. An alternative strategy would be to slightly offset the mirrors from the TGFR end-faces, as shown in Fig. 4b. The higher order modes (shown in light red) will diffract very rapidly from the TGFR end-faces, and, therefore, experience a much reduced feedback. The higher beam quality of the fundamental mode does not diffract as

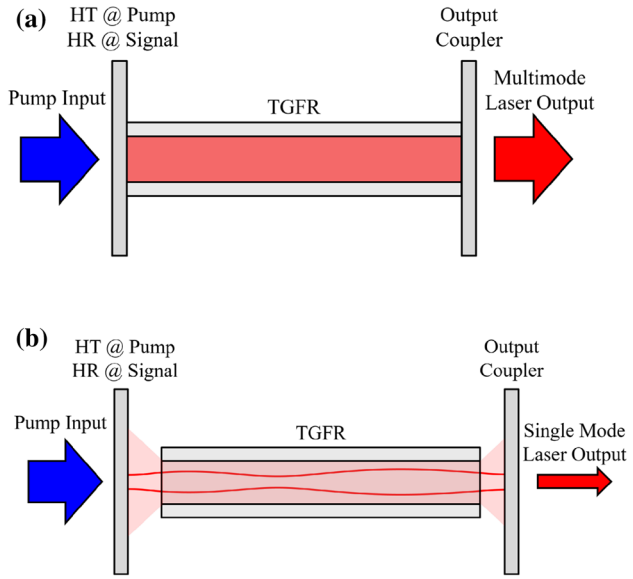

Fig. 4 TGFR operating in a multimode (**a**) and single-mode (**b**) configuration

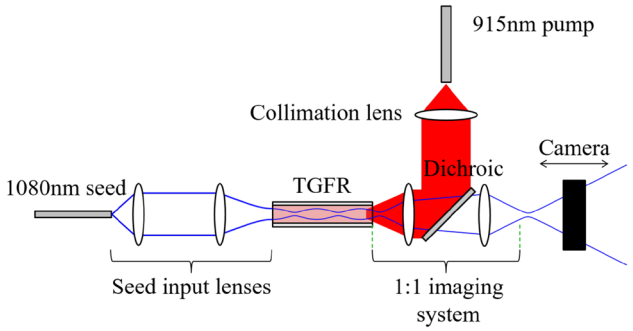

Fig. 5 Experimental setup used to investigate thermal-guiding within the TGFR device

quickly, and thus, through careful cavity design, one can ensure that this mode is effectively fed back into the gain medium. This approach ensures that the fundamental mode reaches threshold first and, therefore, saturates the available gain, leading to single-mode output.

3 Validation of guiding mechanism

To experimentally validate the guiding model, the experimental setup shown in Fig. 5 was employed. In this arrangement, a single-mode probe beam at 1080 nm, provided by a tunable Yb-doped silica fiber laser, was launched into one end of the TGFR with known input beam parameters. A fiber-coupled diode laser operating at 915 nm was launched into the signal output end of the device in a counter-pumping configuration. The pump wavelength was chosen for thermal guiding, amplifier, and laser experiments, since it corresponds to a broad absorption peak for Yb-doped silica. The pump fiber had a core diameter of 105 µm and a core NA of 0.22, and was imaged into the device using an imaging system consisting of collimating lens with a 25 mm focal length and a focusing lens with a 50 mm focal length. This pump configuration creates a beam waist radius of 105 µm, with an NA of 0.11, at the TGFR end-face, satisfying the condition for core guidance. The probe beam is imaged from the output face of the TGFR using a 1:1 imagining system, consisting of two identical lenses of 50 mm focal length separated by 100 mm. Therefore, the beam evolution from the output plane of this imaging system can be considered identical to the beam evolution from the output of the TGFR. Furthermore, one can measure the evolution of the beam radius from the output plane as a function of pump power. This evolution can be used to verify the thermal-guiding principle once the static contribution to guiding has been validated, since we know the input beam parameter, q_{in}, the ABCD matrix, and the output beam parameter, q_{out}. By varying the pump power, we can vary the thermal lens strength in a controllable way. This will change the parameters of each ABCD matrix that makes up the TGFR. Therefore, the accuracy of the model can be determined by comparing the modelled and measured output beam evolution across a range of pump powers. It should be noted that the model takes into account the variation in pump power absorbed per unit length along the fiber-rod gain medium.

Before investigating the effectiveness of the model in predicting thermal-guiding, it was first necessary to calculate the static guiding contribution inherent to the TGFR device, n_s. To investigate this component, we utilise the imaging system depicted in Fig. 5 without launching the pump power, i.e., without inducing any thermal lensing effect.

The beam evolution investigation was conducted on a 59 mm long section of the TGFR. Antireflection (AR)-coated end-caps were spliced onto the end-faces of the TGFR using an in-house splicing system which utilises a CO_2 laser to reach the temperature required for splicing. The AR-coated end-caps reduced the Fresnel losses of the end-faces of the TGFR from approximately 3.4% to $<0.5\%$ across the wavelength range of interest, i.e., 915–1080 nm. An input beam, at 1080 nm, was focused to a waist radius of approximately 78 µm, at a longitudinal position of $z=0$ mm. The longitudinal position of the input face of the TGFR, z_{TGFR}, was shifted relative to the waist position. The output beam evolution was recorded for each value of z_{TGFR}.

The value of n_s was assumed to be longitudinally constant. Since both q_{in} and q_{out} are known, we can scan over a range of n_s to determine the predicted output, and, therefore,

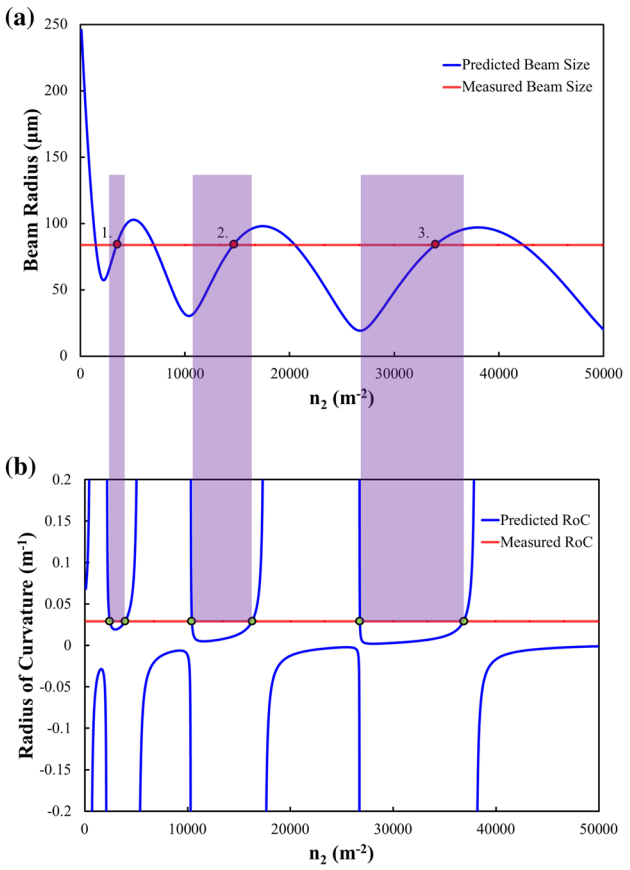

Fig. 6 Output beam size (**a**) and radius of curvature (**b**) as a function of n_2 for $z_{TGFR} = 13$ mm

find the solutions which satisfy our requirements. Figure 6 depicts this process, where we have plotted output beam size and wavefront radius of curvature for $z_{TGFR} = 13$ mm.

We have scanned the output beam parameters for $n_s = 0$–$50{,}000$ m^{-2}, to cover several oscillations of the beam along the length of the device. This can be seen from the oscillating beam size, as the output of the device periodically coincides with a crest or trough of the undulating beam, and also from periodic switching of the radius of curvature from positive (expanding beam) to negative (converging beam). The red lines shown in Fig. 6 correspond to the measured output beam parameters; therefore, the intersection points of the plots indicate values of n_s that will satisfy the output beam parameters. The green circles in the radius of curvature plot indicate the solutions which satisfy the measured values. The red circles in the beam radius plot indicate solutions, whereby the beam radius satisfies the measured value, and the beam has the correct sign for the radius of curvature, which for this example is positive, as the beam is expanding at the output. Here, we note three solutions for the beam size which satisfy these requirements. The purple regions indicate the discrepancy between each of the three solutions and the two nearest solutions for the radius of curvature, i.e., one solution either side. Here, we note that the discrepancy is smallest for the first solution.

This examination technique was applied across the range of z_{TGFR} positions, and it was observed that the solutions tended to centre on the solutions, as shown in Fig. 6. Taking an averaged solution for the region around the first red circle of $n_s = 3600$ m^{-2}, we observed excellent agreement with the measured data. Figure 7 shows the predicted and measured beam evolution for $z_{TGFR} = 13$ mm, whilst Fig. 8 shows predicted and measured beam evolution from the output plane for four z_{TGFR} positions. Due to a lack of a reliable RIP on the TGFR core itself, we are unable to confirm whether the solution from region 1 is in close agreement with the measured profile. However, this solution provides close agreement with the measured beam evolution, and, therefore, allows us to investigate the additional impact of thermal-guiding.

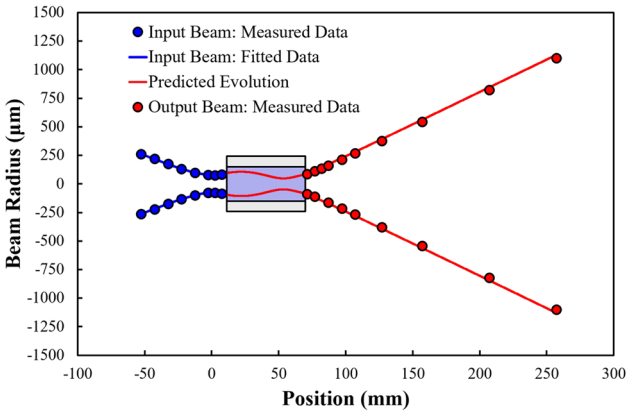

Fig. 7 Measured and predicted beam evolution through the TGFR for $z_{TGFR} = 13$ mm assuming a parabolic RIP with $n_2 = 3600$ m^{-2}

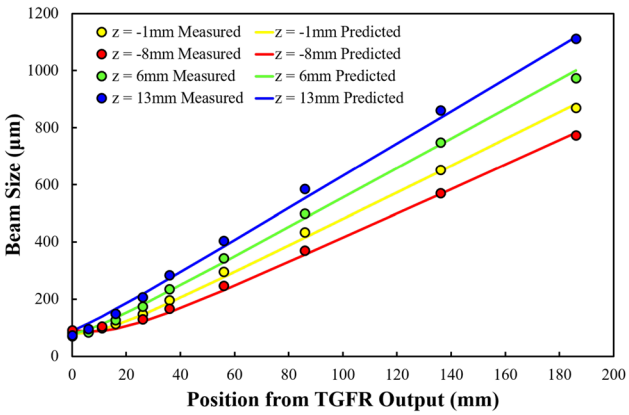

Fig. 8 Measured and predicted beam evolution from TGFR output for $z_{TGFR} = -8$ mm, -1 mm, 6 mm, and 13 mm, assuming a parabolic RIP with $n_2 = 3600$ m^{-2}

The thermal-guiding aspect of the model was then explored on the same TGFR device. In this investigation, a beam at 1080 nm was focused to a waist of approximately 69 µm, with the TGFR positioned at $z_{TGFR} = 5$ mm. These input conditions were kept constant, whilst the launched pump power was varied. Assuming the previously determined solution of $n_s = 3600\ m^{-2}$ and a value for the thermo-optic coefficient of $dn/dT = 12.9 \times 10^{-6}\ K^{-1}$, we observed excellent agreement with the measured data across the full range of pump power, up to a maximum launched/absorbed pump power of 30 W/20 W. The predicted and measured beam evolution for the range of pump powers is shown in Fig. 9. This excellent agreement proves the validity of the thermal-guiding model, confirming it as a powerful tool that can be utilised to optimise amplifier and laser performance.

4 Amplifier investigation

Following the mode control investigation, the TGFR was characterised in terms of amplifier performance. In this section, we experimentally measure gain in the device at 1030 nm. To investigate the single-pass gain within the TGFR device, a similar setup to that used for the mode control investigation was used, as shown in Fig. 5. However, a power meter replaced the camera to determine the output power over a range of pump powers.

The tunable seed laser used for the thermal-guiding experiment was tuned to 1030 nm for the gain investigation. The input beam was focused to a waist radius of approximately 70 µm at the input face, which led to an estimated average beam radius of 60 µm throughout the TGFR, according to the thermal-guiding model. The measured gain values for an input seed power of 50 mW and 1.1 W are shown in Fig. 10 up to a maximum launched pump power of approximately 54 W. A maximum gain of 5.0 dB was achieved for the 50 mW seed resulting in an output power of 160 mW and 3.9 dB for the 1.1 W seed resulting in an output power of 2.7 W.

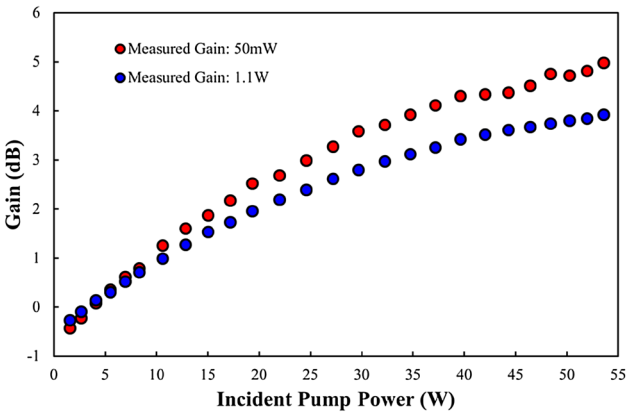

Fig. 10 Measured gain of a 59 mm long TGFR at 1030 nm

The beam quality remained excellent throughout amplification, i.e., $M^2 < 1.1$, over the full range of seed and pump powers. Figure 11 shows the beam quality in the x-direction and beam profile at maximum pump power for the 50 mW beam amplified at the maximum pump power.

The results from the amplifier investigation are encouraging. At present, the single-pass gain is limited by available pump power and fiber-rod length. Both can be scaled in a relatively straightforward manner allowing much better extraction efficiency and thus higher output power. Even without further optimisation, the measured single-pass gain values are more than sufficient for the demonstration of a laser based on the TGFR.

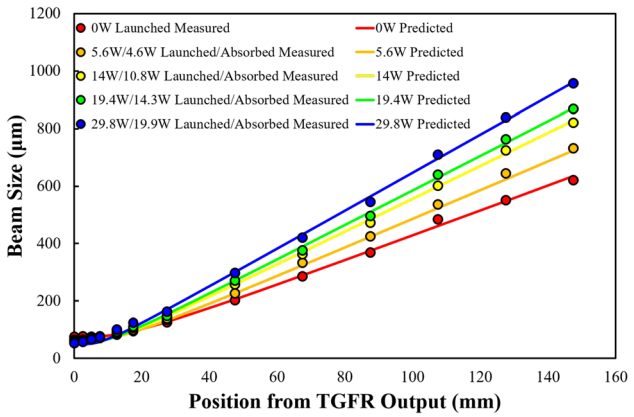

Fig. 9 Measured and predicted beam evolution from the TGFR for various launched pump powers

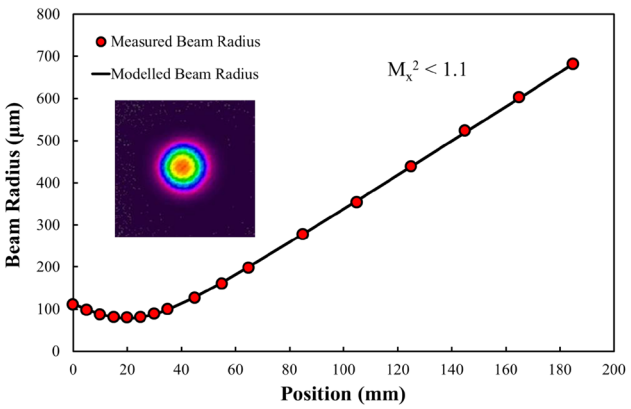

Fig. 11 Beam quality and beam profile for 50 mW at the maximum pump power

5 Laser investigation

The final experimental section of this paper utilises the results obtained thus far to explore the TGFR device in a laser configuration. The guiding investigation informs the design of a stable cavity, whilst the gain performance investigation allows an estimation of threshold powers, thus dictating appropriate intracavity optics.

For a stable resonator mode, we require that the beam profile is self-reproducing. It is useful to be able to predict which cavity configurations are stable, and what the resulting beam size will be throughout the cavity in that configuration. This can be achieved with the guiding mechanism introduced in Sect. 2. For simplicity, a two mirror cavity is considered, as shown in Fig. 12. Here, a plane pump input mirror and a plane laser output mirror are offset from the end-faces of the TGFR by approximately 5 mm. The pump input mirror is highly transmissive at the pump wavelength and highly reflective at 1030 nm (the intended operating wavelength). The laser output mirror has a reflectivity of 70% at 1030 nm. A stable resonator mode must form a waist on the plane mirrors. Therefore, we can stipulate that Eq. 4 simplifies to

$$q = \frac{Aq + B}{Cq + D}. \tag{9}$$

Thus, we can determine the beam parameters at the mirrors for a given pumping configuration. Following this, we can propagate the beam through the TGFR as before to establish the beam parameters at each position. Figure 12 shows the modelled beam evolution for a launched/absorbed pump power of 50 W/27.5 W taking into account the decrease in pump absorption per unit length along the fiber rod. An important feature worth emphasising is that the beam size evolves in a relatively slow manner (i.e., without any abrupt increase in size or divergence), even though the heat generated per unit length decreases by more than a factor-of-two over the length of the fiber-rod. This configuration gave an average beam size through the TGFR of approximately 75 µm.

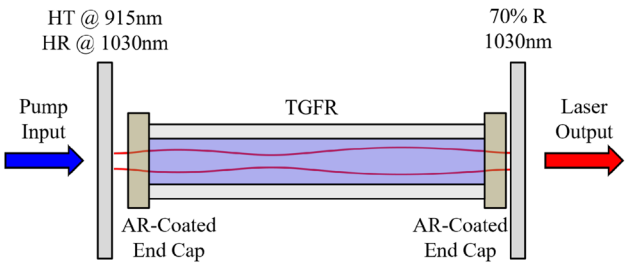

Fig. 12 Configuration for laser investigation

The cavity was optimised for maximum output power. Threshold was reached at approximately 14 W of launched pump power. A maximum output power of 13.1 W was achieved, with a corresponding maximum slope efficiency of 44%/53% with respect to launched/absorbed power, as shown in Fig. 13. Note that the slope efficiency increases, as the laser is operated further above threshold, owing to the laser radiation saturating gain more effectively in the beam wings. The slope efficiency with respect to absorbed power, 53%, is reasonable, with the theoretical limit for this transition approaching 89% with a perfect overlap between pump and laser mode. In addition, one would expect the slope efficiency to improve by operating the laser further above the threshold power.

Figure 14 shows the wavelength spectrum at maximum output power. The wavelength spectrum is fairly broad with several peaks. This is not surprising considering that no wavelength selection was employed in this configuration. The main peak is centred on 1032.5 nm with an FWHM of 1.3 nm.

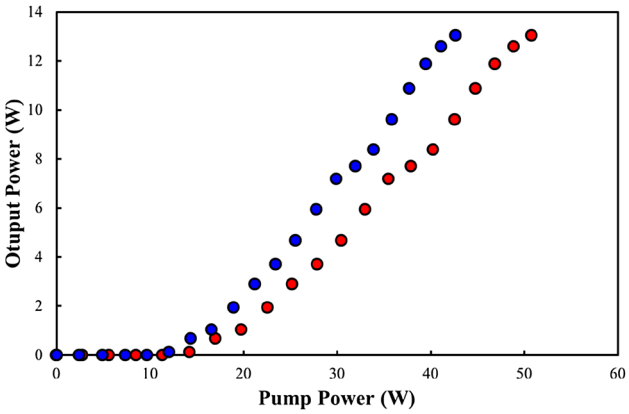

Fig. 13 Output power as a function of launched and absorbed power

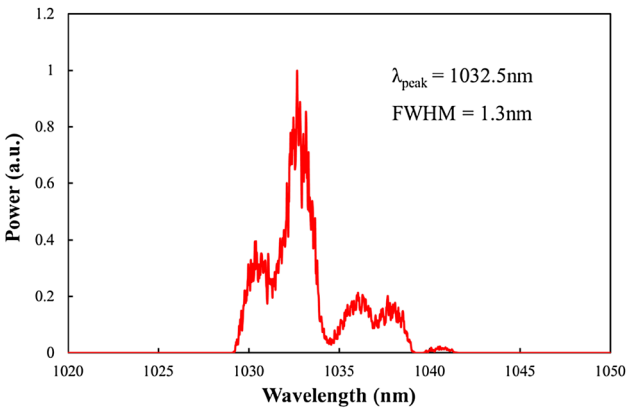

Fig. 14 Output wavelength at maximum pump power

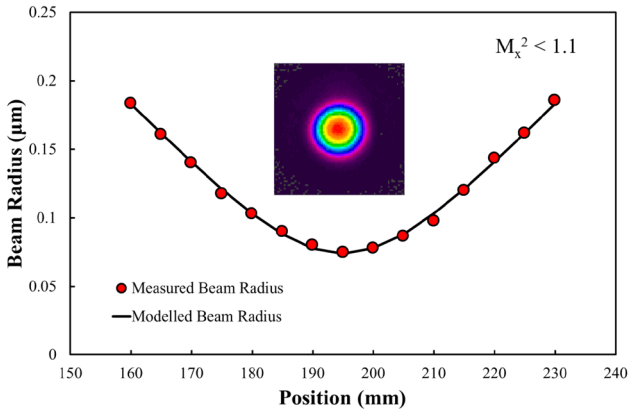

Fig. 15 Beam quality and beam profile at maximum pump power

Excellent beam quality was achieved at maximum output power with $M^2 < 1.1$. Figure 15 shows the beam quality in the x-direction and the beam profile at maximum pump power. This result confirms that non-parabolic phase distortion, due to the non-uniform radial pump profile, is negligible at the power levels under consideration here. At higher power levels, the use of a cladding-pumped architecture would lead to a more uniform radial pump deposition and help mitigate unwanted beam distortion. This is in contrast to the situation in a crystal fiber gain medium, where the absence of a cladding means that the thermal load extends edge of the medium, making it difficult to avoid non-parabolic phase aberration.

6 Conclusion

In this paper, we have introduced and demonstrated the concept of the TGFR using an extra-large-mode-area ytterbium-doped silica fiber. In Sect. 2, a guiding mechanism was suggested which utilises a thermal and static parabolic refractive index profile to control mode size. Section 3 investigated this model experimentally, first calculating the strength of the static contribution followed by a validation of the thermally induced guiding mechanism. This confirms the value of the guiding model as a tool for predicting beam evolution through the TGFR. Section 4 investigates the performance of the TGFR as an amplifier for a seed beam at 1030 nm up to a maximum launched pump power of 54 W. A maximum gain of 5.0 dB was achieved for a 50 mW seed resulting in an output power of 160 mW, and 3.9 dB for a 1.1 W seed resulting in an output power of 2.7 W. Excellent beam quality was maintained throughout amplification with $M^2 < 1.1$. The obtained results were then utilised to investigate the performance of the TGFR as a laser in Sect. 5. The mode control investigation was used to construct a model for predicting laser resonator stability. The model can predict how the fundamental mode would propagate in an arbitrary cavity, which for this investigation was a simple cavity with plane mirrors approximately 5 mm from the TGFR end-faces. The laser, operating at 1032.5 nm, reached threshold at 14 W and achieved a maximum output power of 13.1 W with a slope efficiency of 44%/53% with respect to launched/absorbed pump power. Excellent beam quality was achieved at maximum output power with $M^2 < 1.1$.

In future work, we aim to achieve a higher efficiency by operating with a higher pump power and improved end-cap AR coatings. One important design aspect of the TGFR is that the heat loading per unit length should not fall to zero at the end of the fiber-rod. Thus, achieving high overall pump absorption efficiency and maintaining thermal guiding require a double-pass pumping configuration or pumping from both ends of the fiber rod. We also aim to investigate this geometry in a pulse regime. As pump power increases, the optimum guided mode size will decrease (Eq. 7); therefore, a longer device with a lower heat load per unit length will be desirable. This can be achieved by lowering the doping concentration in the core of the TGFR, or using cladding pumping, to reduce the overlap factor between the pump radiation and the core region. This strategy will allow the heat load per unit length to be kept at a reasonable value, whilst the total power extracted from the device can be increased whilst maintaining a large-mode size consistent with a high damage limit and suppression of unwanted nonlinear processes.

Acknowledgements The authors acknowledge support from Fianium and the Engineering Physical Sciences Research Council (EPSRC) for an Industrial CASE studentship. The authors thank Dr. Adrian Carter of Coherent/Nufern.

Data availability The data underpinning this publication is available from the University of Southampton repository at https://doi.org/10.5258/SOTON/D0797.

References

1. H. Bruesselbach, D.S. Sumida, IEEE J. Sel. Top. Quantum Electron. **11**, 600 (2005)
2. H.J. Eichler, A. Haase, R. Menzel, IEEE J. Quantum Electron. **31**, 600 (1995)
3. E. Stiles, in *Proceedings of the 5th International Workshop on Fiber Lasers*, 30 September–1 October 2009, Dresden, Germany (2009)

4. Y. Jeong, J.K. Sahu, D.N. Payne, J. Nilsson, Opt. Express **12**, 6088 (2004)
5. T. Eidam, S. Hanf, E. Seise, T.V. Andersen, T. Gabler, C. Wirth, T. Schreiber, J. Limpert, A. Tunnermann, Opt. Lett. **35**, 94 (2010)
6. T. Eidam, J. Rothhardt, F. Stutzki, F. Jansen, S. Hadrich, H. Carstens, C. Jauregui, J. Limpert, A. Tunnermann, Opt. Express **19**, 255 (2011)
7. X. Delen, S. Piehler, J. Didierjean, N. Aubry, A. Voss, M.A. Ahmed, T. Graf, F. Balembois, P. Georges, Opt. Lett. **37**, 2898 (2012)
8. F. Jansen, F. Stutzki, H. Otto, C. Jauregui, J. Limpert, A. Tünnermann, Opt. Lett. **38**, 510 (2013)
9. J. Cao, W. Liu, H. Ying, J. Chen, Q. Lu, Laser Phys. **28**, 035106 (2018)
10. M. Leich, F. Just, A. Langner, M. Such, G. Schotz, T. Eschrich, S. Grimm. Opt. Lett. **36**, 1557 (2011)
11. W. Koechner, *Solid-State Laser Engineering*. Springer Series in Optical Sciences, 4th edn. (Springer, New York, 1996)
12. D.C. Brown, H.J. Hoffman, IEEE J. Quantum Electron. **37**, 207 (2001)
13. T. Toyoda, M. Yabe, J. Phys. D Appl. Phys. **16**, L97 (1983)